




Multi-color UCNPs/CsPb(Br_{1-x}I_x)₃ for upconversion luminescence and dual-modal anticounterfeiting

MINGXING LI,^{1,†} WENTING LIU,^{1,†} TIESHAN YANG,^{2,†} QINFENG XU,^{1,*} HAIFENG MU,^{1,3} JING HAN,¹ KUNJIAN CAO,¹ MENG MENG JIAO,¹ MINGLIANG LIU,¹ SHUFANG ZHANG,¹ XIAOMING TAN,^{1,4} AND CHUANLU YANG^{1,5} 

¹Department of Physics and Optoelectronic Engineering, Ludong University, Yantai 264025, China

²School of Mathematical and Physical Sciences and the ARC Centre of Excellence for Transformative Meta-Optical Systems (TMOS), Faculty of Science, University of Technology Sydney, Ultimo, New South Wales 2007, Australia

³hai-fengmu@163.com

⁴mingtanxiao@163.com

⁵yangchuanlu@126.com

[†]Co-first Authors

*xuqf5678@163.com

Abstract: Advanced hybrid materials have attracted extensive attention in optoelectronics and photonics application due to their unique and excellent properties. Here, the multicolor upconversion luminescence properties of the hybrid materials composed of CsPbX₃ (X = Br/I) perovskite quantum dots and upconversion nanoparticles (UCNPs, core-shell NaYF₄:25%Yb³⁺,0.5%Tm³⁺@NaYF₄) is reported, achieving the upconversion luminescence with stable and bright of CsPbX₃ perovskite quantum dots under 980 nm excitation. Compared with the nonlinear upconversion of multi-photon absorption in perovskite, UCNPs/CsPbX₃ achieves lower power density excitation by using the UCNPs as the physical energy transfer level, meeting the demand for multi-color upconversion luminescence in optical applications. Also, the UCNPs/CsPbX₃ combined with ultraviolet curable resin (UVCR) shows excellent water and air stability, which can be employed as multicolor fluorescent ink for screen printing security labels. Through the conversion strategy, the message of the security labels can be encrypted and decrypted by using UV light and a 980 nm continuous wave excitation laser as a switch, which greatly improves the difficulty of forgery. These findings provide a general method to stimulate photon upconversion and improve the stability of perovskite nanocrystals, which will be better applied in the field of anti-counterfeiting.

© 2023 Optica Publishing Group under the terms of the [Optica Open Access Publishing Agreement](#)

1. Introduction

Counterfeiting and forgery is a global, long standing problem that causes significant negative impacts on the social economy and poses security threats to individuals, companies, and society [1,2]. Traditional anti-counterfeiting labels, such as watermarks or holographic patterns have limited coding capacity and are easy to replicate, which makes the correspondingly protected products vulnerable to counterfeiting. In contrast, chemical anti-counterfeiting methods make the counterfeiting very technically demanding due to their advantages of high selectivity, short read time, and the easy chemical detection characteristics [3]. During the past years, various fluorescent materials, including organic dyes [4], carbon dots [5,6], inorganic quantum dots [7,8], upconversion nanoparticles (UCNPs) [9,10], and perovskite quantum dots (PeQDs) [11], have been used in data encryption.

Rare earth doped UCNPs as one of the new type of optical materials, with the behavior of transforming near-infrared (NIR) light to ultraviolet (UV) or visible (VIS) light due to their high multiphoton absorption efficiency under NIR excitation, as well as high stability, large anti-Stokes shift, and narrow emission bandwidth, has drawn much attention in diverse functional applications during the past several years [12–23]. As one of the security strategies in anti-counterfeiting applications, UCNPs are widely used in currencies and documents. The common anti-counterfeiting material in practical application is Yb:Tm/Er co-doped crystal with fluorescence emission [24–27]. However, these upconversion luminescence (UCL) anticounterfeiting materials can exhibit nearly unchanged color under excitation, resulting in a constructed security pattern that is likely to be imitated by using other substitutes with the similar emission.

All-inorganic PeQDs have excellent physicochemical properties, such as large absorption coefficient, high photoluminescence quantum yield (PLQY), and various PL emission by changing halide composition [28,29]. These unique properties enable them to emerge as promising optically active materials for potential applications in anti-counterfeiting. However, PeQDs are sensitive to temperature, humidity, and UV light, which limits their implications in a long-time scale. Meanwhile, the absorption capacity of PeQDs for NIR light is insufficient, although they have a large absorption cross-section in the blue light region. The poor absorption of the NIR light of PeQDs is due to the poor multi-photon absorption ability and the lack of intermediate energy levels for energy transfer. Rare earth doped perovskite can use rare earth ions as energy transfer level, but this way is usually used for down-conversion luminescence of perovskite [30–32]. To realize the two-photon upconversion of perovskite, the excited laser needs to have a strong energy density. However, the price of the NIR pulse laser is usually expensive.

Combined with the unique characteristics of the two kinds of nanoparticles of UCNPs and PeQDs, multicolor luminescence and high-efficiency infrared absorption can be achieved by the composition of the UCNPs and PeQDs. Recently, several studies to achieve upconversion fluorescence based on the combination of PeQDs and UCNPs have been reported [33–37]. In this energy transfer process, UCNPs is the energy donor and PeQDs is the energy acceptor in the process of energy transfer. According to the coupling degree, the UCL mechanism can be divided into Förster resonance energy transfer (FRET) or emission reabsorption (ERA). When the distance between the molecules is greater than the limit of energy transfer, UCNPs will release high energy photons, absorbed by PeQDs to emit its fluorescence. When the molecules are close enough, heterostructures will be formed that allow electrons to be transferred from UCNPs to PeQDs without radiation. The FRET of the UCNPs/PeQDs is deeply affected by the degree of the molecular coupling, which usually leads to low efficiency of perovskite band transition. In contrast, the ERA strategy shows stronger fluorescence emission due to the excellent optical absorption ability of PeQDs. Notably, the upconversion efficiency of the ERA mechanism depends on the luminescence efficiency of PeQDs. It cannot be neglected that the inherent vulnerability of perovskite makes PeQDs decompose rapidly in polar solvent, humid, light, and heating conditions [38,39]. Environmental stability has become a major issue for PeQDs, limiting their further practical applications. One of the feasible strategies to overcome the poor stability of the PeQDs is polymer encapsulation, which provides more resistance against environmental factors than many other attempts of embedding them into mesoporous materials or silane [40,41]. Some polymers, such as polymethyl methacrylate (PMMA) [42] and polyvinylidene fluoride (PVDF) [43], have been proven to provide sufficient protection to PeQDs. These ways provide a great opportunity to use PeQDs in fluorescence-based upconversion encryption.

Herein, we propose a rational design strategy to fabricate uniform UCNPs/CsPbX₃ (X = Br/I) hybrid materials for achieving the unique UCL under 980 nm continuous wave (CW) laser. The UCNPs/CsPbX₃ hybrid materials are produced by mixing two kinds of nanoparticles in different ratios and combine the advantages of each nanoparticle, including excellent infrared absorption and multi-color fluorescence. Correspondingly, the ultraviolet curable resin (UVCR)

has excellent flexibility and crack resistance, and can be polymerized in a short time under UV light. The UCNPs/CsPbX₃@UVCR nanocomposite obtained by combining UCNPs/CsPbX₃ hybrid materials with UVCR has excellent water and air stability. Compared with other packaging methods, the UVCR encapsulation eliminates the operation of high temperature molding and volatilization of harmful gases, which better protects the complete crystal structure of nanoparticles. In addition, the UCNPs/CsPbX₃@UVCR nanocomposites as fluorescent ink inherits a certain viscosity of the resin, and can be prepared into anti-counterfeiting labels by screen printing. Under the excitation of UV light and 980nm laser respectively, the anti-counterfeiting label with multi-channel emission has different color response, which greatly increases the difficulty of counterfeiting. Through the conversion strategy, different message of the anti-counterfeiting label can be interpreted by using the excitation light as the switch, which shows its potential application value in the field of optical security.

2. Results and discussion

High quality CsPbBr₃ PeQDs were synthesized through a facile and classical method by injecting the precursor of Cs-oleate to Pb(II) solution at an elevated temperature. Morphology and size distribution of the synthesized PeQDs are analyzed using TEM and HR-TEM. As shown in Fig. 1a and Fig. 1b, the CsPbBr₃ PeQDs exhibit a uniform monodisperse cubic structure, which corresponds to the XRD pattern well. The HR-TEM image exhibits a well-crystallized structure with a lattice fringe spacing of 0.58 nm, which is consistent with the spacing of the (100) plane in cubic CsPbBr₃ (see Fig. S2 in the Supplementary document. The diffraction peaks of X-ray diffraction (XRD) located at $2\theta = 15.3^\circ, 21.2^\circ, 30.4^\circ, 37.6^\circ, \text{ and } 44.1^\circ$ can be assigned to the crystal planes (1 0 0), (1 1 0), (2 0 0), (2 1 1) and (2 2 0) of CsPbBr₃, respectively). In addition, the NaYF₄: 25%Yb³⁺, 0.5%Tm³⁺ nanoparticles are produced through high-temperature coprecipitation in a dual solvent mixture of oleic acid and 1-octadecene. Lanthanide co-doping can be achieved during particle growth by controlling the composition and concentration. The lanthanide doped NaYF₄ nanoparticles then serve as seed crystals for subsequent epitaxial growth of shell layers. From Fig. 1(d) and Fig. 1(e), we can confirm that the core-shell hexagonal NaYF₄: 25%Yb³⁺, 0.5%Tm³⁺@NaYF₄(UCNPs) have pure phase and high crystallinity. Considering the histogram of particle size distribution (Fig. 1c and Fig. 1f), the average diameter of CsPbBr₃ and UCNPs is 11.56 nm and 30.02 nm, respectively. From these above-mentioned data, it is proved that the two kinds of nanoparticles have standard material structure.

To test the UCL properties of the hybrid nanoparticles, we mixed the two nanoparticles of UCNPs and PeQDs in different proportions. The mixing of nanoparticles can make full use of the advantages of both UCNPs and PeQDs. In the process of energy transfer from UCNPs to PeQDs (Fig. 2), UCNPs acts as energy donor, absorbing NIR 980 nm laser and emitting high-energy photons (¹D₂-³F₄, 450 nm; ¹G₄-³H₆, 476 nm), while CsPbBr₃ acts as energy receptor reabsorbing high-energy photons and emitting own fluorescence. Yb³⁺ is a perfect sensitizer for NIR light at 980 nm due to their large absorption cross-sections. Notably, the higher concentration of rare earth ions can cause cross relaxation and reduce the UCL efficiency, which sets a barrier for improving the energy transfer efficiency by increasing the concentration of doped ions to shorten the distance between rare earth ions. However, only one energy level ²F_{5/2} possessed by Yb ion is not restricted by the doping concentration. The UCL benefits from the doping of high concentration Yb³⁺ in UCNPs (≥ 20%), which makes the energy transfer from Yb ion to Tm ion more efficient. In addition, PeQDs is also an excellent material with unique optical properties. In the upconversion system, PeQDs play the role of the energy output terminal, responsible for the collection and conversion of high-energy photons. The significant quantum size effect enhances the coherence and localization of electrons in PeQDs, which greatly improves the optical absorption capacity of PeQDs excitons. Therefore, the large absorption cross section in

the blue region and the excellent PL ability is possessed by PeQDs, which further promotes the upconversion capability.

The PL and UV–VIS absorption spectra of the synthesized CsPbBr₃ PeQDs are illustrated in Fig. 3(a). The PL emission peak of the CsPbBr₃ PeQDs is located at 520 nm with a FWHM of 21.8 nm and a PLQY of 84% is obtained in a toluene solution. The bright green emission is ascribed to the band-edge exciton recombination over the entire visible spectral region [44]. PL decays indicate that effective PL lifetime of the band-edge excitons is about 18.8 ns (Fig. 3(b)). Under CW 980 nm excitation (Fig. 3(c)), the UCNPs shows intense UCL with a set of sharp and typical emission peaks from Tm³⁺, which are divided into three regions: the blue region with peaks at 450 nm (¹D₂-³F₄) and 476 nm (¹G₄-³H₆), the green region with peak at 510 nm (¹D₂-³H₅), as well as the red region with single peak at 648 nm (¹G₄-³F₄) (see Fig. 2 for a simplified diagram of transitions in the Yb³⁺-Tm³⁺ system). As a comparison, the UCNPs/CsPbBr₃ hybrid materials show bright UCL at a central wavelength of 520 nm, accompanied by a large decrease in the blue peak regions of 450 nm (¹D₂-³F₄) and 476 nm (¹G₄-³H₆). Apparently, the luminescence mode of composite UCNPs/CsPbBr₃ follows the process of ERA [33,45]. As shown in Fig. 3(d), the PL lifetime is extended to 0.75 ms at the wavelength of 520 nm, indicating that the PeQDs luminescence in UCNP/PeQDs upconversion system is a delayed process under 980 nm excitation. During the upconversion luminescence process, the time scale of the total fluorescence lifetime is no longer dominated by the band-edge exciton lifetime of PeQDs, but becomes the linear sum of PeQDs and Tm³⁺ fluorescence lifetime. Under 980 nm excitation, Tm³⁺ lifetime decay is the main part of the total lifetime decays process, so the UCL decays of UCNPs/CsPbBr₃ reveal a similar temporal distribution as Tm³⁺, namely, a rising edge in the initial stage followed by single exponential decay, as a result of the ERA process. The extended lifetime of UCNPs/CsPbBr₃ reflects the correlation of the luminescence process of hybrid materials, which has a potential application in the field of lifetime imaging and infrared detection [46].

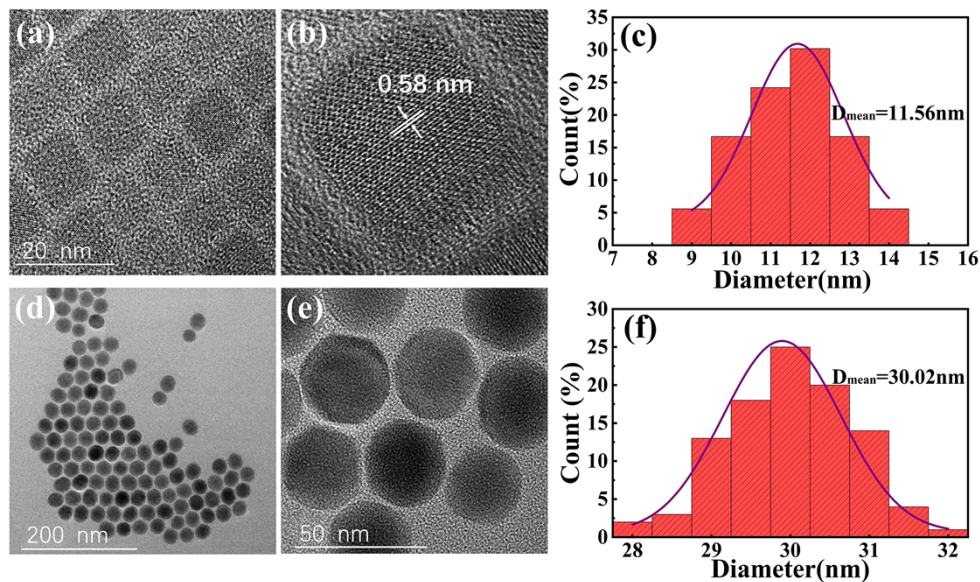


Fig. 1. (a)TEM, (b) HR-TEM images, and (c) particle size distribution of CsPbBr₃ PeQDs. (d) TEM, (e) TEM magnified image, and (f) particle size distribution of core-shell NaYF₄:25%Yb³⁺,0.5%Tm³⁺@NaYF₄ (UCNPs). TEM, Transmission electron microscopy; HR-TEM, High-resolution transmission electron microscopy.

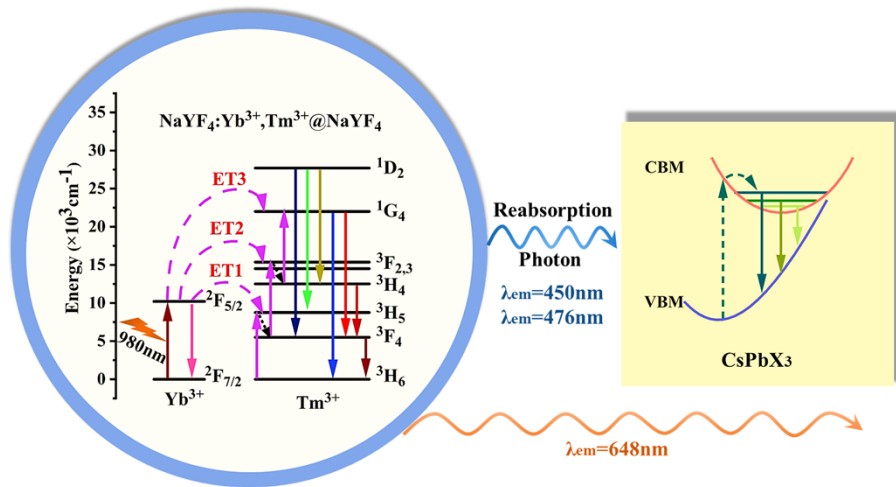


Fig. 2. Schematic diagram of energy transfer mechanism from UCNPs to PeQDs. Under the excitation of a 980 nm laser, UCNPs emit high-energy photons, which are reabsorbed by PeQDs through ERA mechanism and release fluorescence.

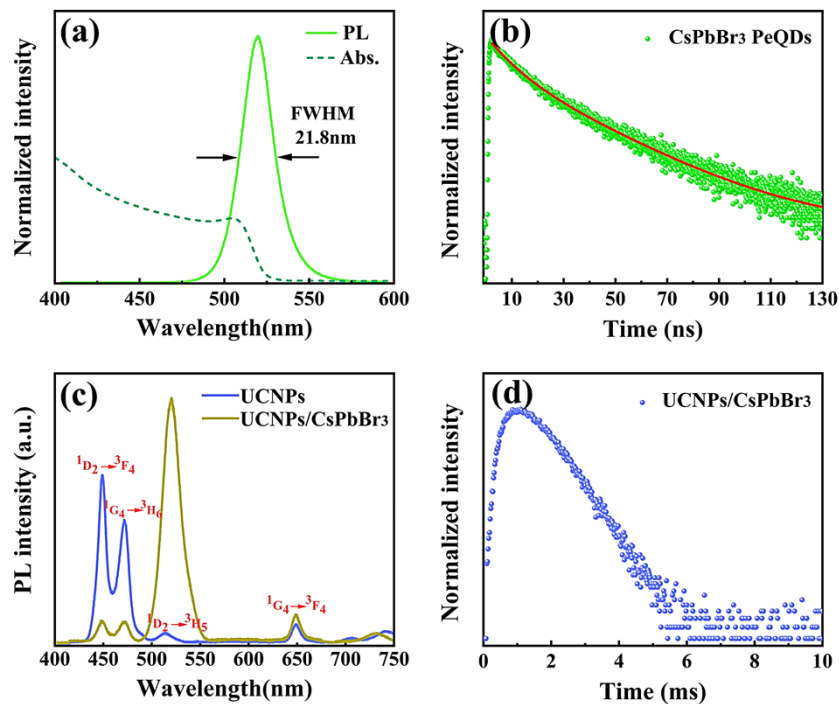


Fig. 3. (a) The PL and absorption spectra of CsPbBr₃ PeQDs. (b) Time-resolved fluorescence decay of the as-synthesized CsPbBr₃ PeQDs ($\lambda_{ex}=405$ nm). (c) The PL spectra of UCNPs (blue line) and UCNPs/CsPbBr₃ (green line) under continuous wave (CW) 980 nm excitation. (d) Time-resolved fluorescence decay of UCNPs/CsPbBr₃ under 980 nm excitation (monitored at the emission of 520 nm).

The energy transfer process is further studied by a series of UCNPs/CsPbBr₃ pairs with different mass ratios. With gradually increasing the ratios of the UCNPs/CsPbBr₃, the energy transfer of UCNPs/CsPbBr₃ is obviously improved. As shown in Fig. 4(a), the emission of CsPbBr₃ at 520 nm increased gradually under 980 nm laser excitation. As expected, the blue emissions of Tm³⁺ are dramatically quenched due to the reabsorption process from UCNPs to CsPbBr₃ PeQDs. The integrated emission intensity of CsPbBr₃ PeQDs (acceptors) at 520 nm shows an increasing trend when the ratio of UCNPs/CsPbBr₃ pairs varies from low to high values (Fig.4b). Meanwhile, the integrated blue emission of Tm³⁺ at 450 nm (¹D₂-³F₄) and 476 nm (¹G₄-³H₆) almost completely disappears, indicating 100% ERA efficiency when UCNPs/PeQDs ratio is 1:2. It can be seen that the red emission at 648 nm does not change with the increase of CsPbBr₃ PeQDs concentration, which further proves that the energy transfer of the system is an ERA process rather than a non-radiative FRET energy transfer. In the luminescence process of UCNPs, the ¹G₄ level transition is divided into two parts, 476 nm (¹G₄-³H₆) and 648 nm (¹G₄-³F₄), respectively. As the receptor content increased, the blue fluorescence intensity at 476 nm gradually decreased, while the red fluorescence intensity did not change at 648 nm, which should not be the result of energy transfer by non-radiative FRET. It should be noted that reducing the ¹G₄ of Tm³⁺ launch channel by non-radiative FRET will result in a simultaneous quenching of all ¹G₄ launches [33,47]. Obviously, the energy transfer reabsorption explanation from UCNPs to CsPbBr₃ PeQDs is more reasonable, which is because the absorption coefficient of CsPbBr₃ PeQDs in blue light is much higher than that in red light. In addition, UCNPs are encased in a shell about 5nm thick (see Fig. S1a in the Supplementary document), which is unfavorable for distance-dependent FRET energy transfer. As shown in Fig. 4(c), the position and shape of upconversion fluorescence peaks of UCNPs/CsPb(Br_{1-x}/I_x)₃ solution are consistent with UV-excited CsPb(Br_{1-x}/I_x)₃, indicating its excellent multicolor upconversion luminescence ability. It should be noted that the weak absorption of 648 nm by PeQDs results in its presence in most of the emission spectrum. During the UCL process, UCNPs can provide blue emission, while CsPb(Br_{1-x}/I_x)₃ can provide green to red emission. The luminescent color of UCNPs/CsPb(Br_{1-x}/I_x)₃ can be controlled by the mass ratio of nanoparticles and the molar ratio of Br/I, fulfilling the RGB color requirement to achieve polychromatic gamut coverage(Fig. 4(d)).

The stability of the UCNPs/CsPbBr₃ hybrid materials is a major limiting factor for further practical applications. As known, CsPbX₃ PeQDs have unsatisfying stability towards water treatment and it has been proved that the degradation can be mitigated when embedding them in UVCR [48]. Thus, the UCNPs/CsPbBr₃@UVCR nanocomposites with excellent stability was obtained by fully mixing the UCNPs/CsPbBr₃ hybrid materials with the UVCR. To obtain the UCNPs/CsPbBr₃@UVCR film, the mixture was dropped on the glass slide and then cured under UV lamp for a short time, as shown in Fig. 5(a). The UCNPs/CsPbBr₃@UVCR films prepared by this method have high transmittance and flexibility, and meet the basic requirements of luminous composites. In addition, UCNPs/CsPbBr₃@UVCR films can be quickly formed at room temperature, making it easier to operate and more conducive to protecting the crystal structure of nanoparticles.

To show the stability of the UCNPs/CsPbBr₃@UVCR film, a contrast sample (original UCNPs/CsPbBr₃ film) was synthesized. Water was dropped onto the surface of the UCNPs/CsPbBr₃@UVCR film and the original UCNPs/CsPbBr₃ film at room temperature, respectively. The normalized PL intensity as a function of the time for original UCNPs/CsPbBr₃ (1:0.25) film and UCNPs/CsPbBr₃@UVCR film stored in water are shown in Fig.6a and Fig.6b, respectively. It can be observed that the PL intensity at a wavelength of 520 nm of UCNPs/CsPbBr₃ nanocomposites decreased sharply after immersion in water. After a while, the green light emission almost disappeared completely, leaving only the fluorescence emission of Tm³⁺(¹D₂-³F₄,450 nm; ¹G₄-³H₆,476 nm). This result indicates poor stability of CsPbBr₃ PeQDs in water. For comparison, the UCNPs/CsPbBr₃@UVCR film possesses outstanding water stability,

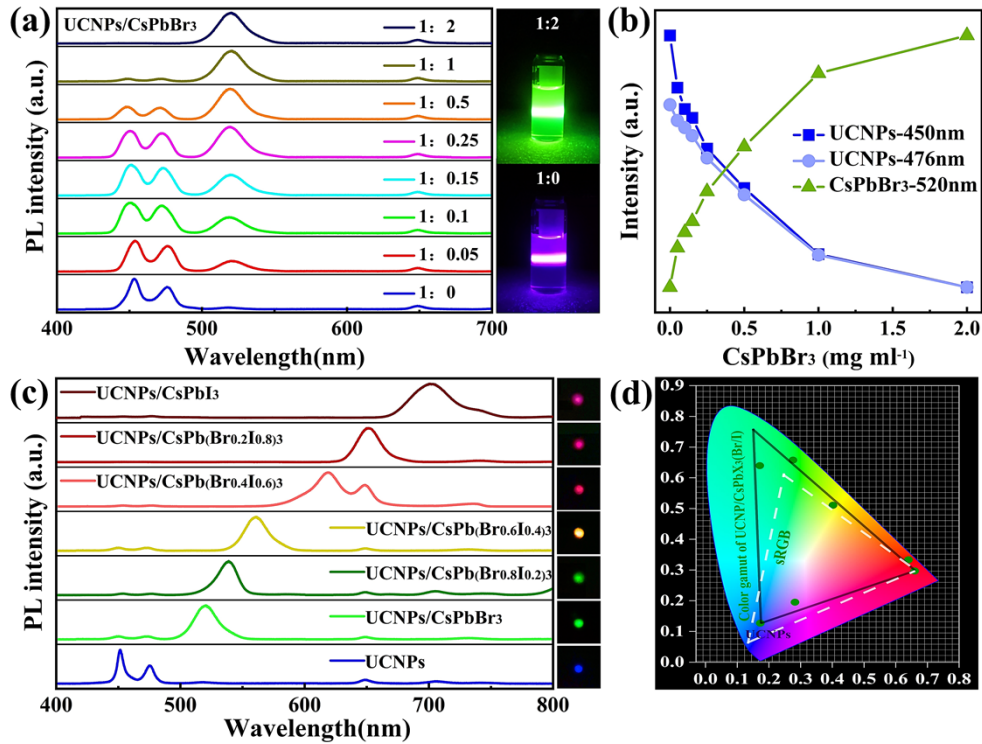


Fig. 4. (a) UCL spectra of UCNP/CsPbBr₃ pairs (1:0, 1:0.05, 1:0.1, 1:0.15, 1:0.25, 1:0.5, 1:1 and 1:2) with varying density of CsPbBr₃ PeQDs excited at 980 nm laser (The attached figure shows the luminescence photos of UCNP/CsPbBr₃ solution at the ratio of 1:0 and 1:2, respectively). (b) Integrated intensities of the Tm³⁺ emissions at 450 nm, 476 nm and the CsPbBr₃ emission at 520 nm vs. the CsPbBr₃ concentration. (c) The corresponding UCL spectra of CsPb(Br_{1-x}I_x)₃ with varying halide compositions under 980 nm laser excitation (Inset figures display the spot color change of CsPb(Br_{1-x}I_x)₃ under 980 nm excitation). (d) Corresponding UCL color gamut of CsPb(Br_{1-x}I_x)₃ nanocomposites (solid black triangle) and compared with most common color standards (sRGB, dashed white triangle).

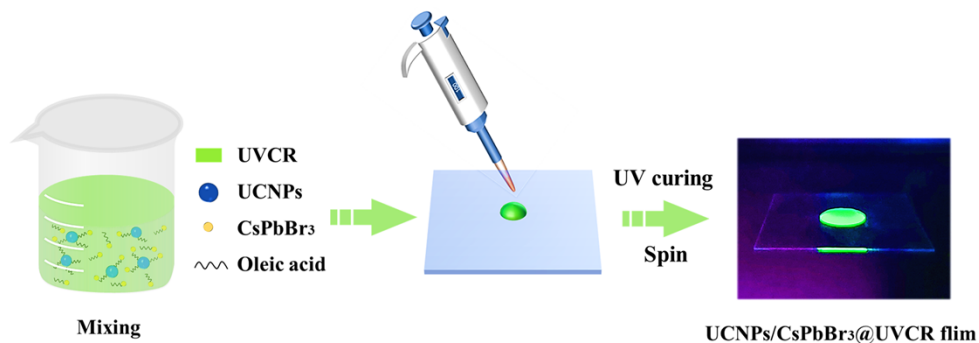


Fig. 5. Schematic diagram of preparation method of UCNP/CsPbBr₃@UVCR. After spinning and UV curing, UCNP/CsPbBr₃@UVCR films can be obtained.

and the relative intensity can maintain above 90% of initial value even after immersed in a water environment. The PL relative intensity spectra are shown in Fig.6c. Obviously, the stability of CsPbBr₃ has been greatly improved after UVCR packaging. Also, the air stability of UCNPs/CsPbBr₃@UVCR was also investigated at room temperature and the PL spectra were recorded. As shown in Fig. 6(d), the PL intensity of the UCNPs/CsPbBr₃@UVCR maintained relatively steady output with 6% fluorescence quenching of the initial PL intensity after a week. The abovementioned results indicate that UCNPs/CsPbBr₃@UVCR mixture possess excellent water and air stability, which are essential for application as fluorescent anti-counterfeiting inks.

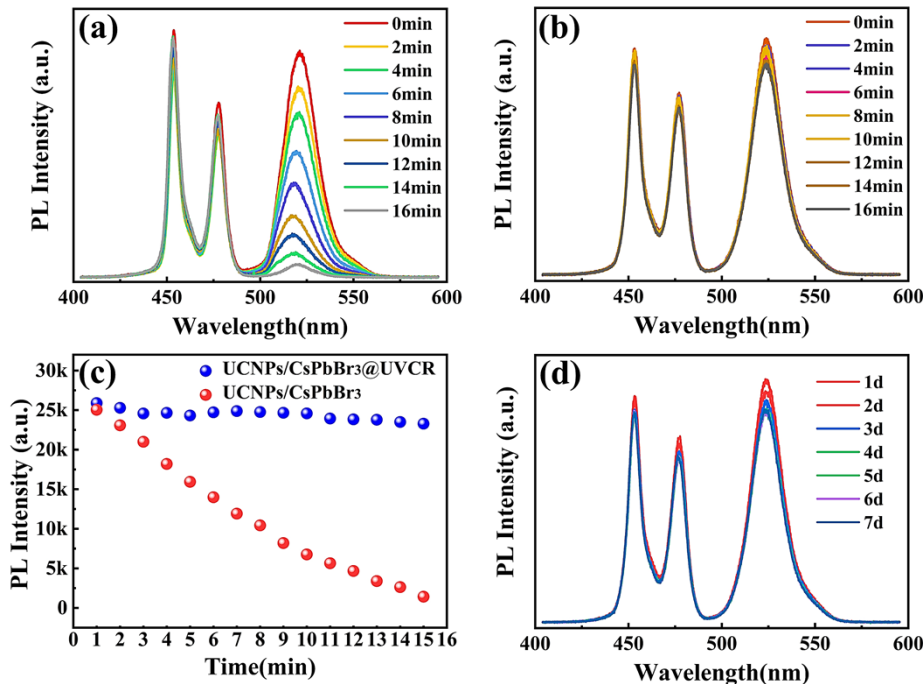


Fig. 6. PL intensity test is used to monitor the stabilities of (a) UCNPs/CsPbBr₃ (UCNPs/CsPbBr₃=1:0.25) and (b) the UCNPs/CsPbBr₃@UVCR in the water. (c) Relative PL intensity of UCNPs/CsPbBr₃ (red) and UCNPs/CsPbBr₃@UVCR (blue) as a function of time. (d) PL intensity test was used to monitor the stability of the UCNPs/CsPbBr₃@UVCR in the air atmosphere.

The application of the UCNPs/CsPbBr₃@UVCR nanocomposites in dual-mode anti-counterfeiting is verified. We designed an anti-counterfeiting pattern through screen printing, as shown in Fig. 7(a). The anti-counterfeiting label is composed of UCNPs/CsPbBr₃@UVCR nanocomposites of appropriate proportions and cured under UV light. Under different excitation, the anti-counterfeiting label appears bright green and cyan respectively due to the different launch channels. At 365 nm excitation, the fluorescence is derived from the intrinsic exciton emission of the PeQDs, whereas at 980 nm excitation, the color of fluorescence is a mixture of upconversion fluorescence and UCNPs blue fluorescence. Figure 7(b) and Fig. 7(c) show the spectra of anti-counterfeiting pattern under laser excitation at 365 nm and 980 nm, respectively. It is worth mentioning that the fluorescence intensity did not decrease significantly after a period of exposure to the natural environment. Taken together, the UCNPs/CsPbBr₃@UVCR inks with quick-drying character, excellent water-resistance as well as dual-modal luminescence, and this dual modal will greatly enhance the safety of code technologies in anti-counterfeiting and authentication.

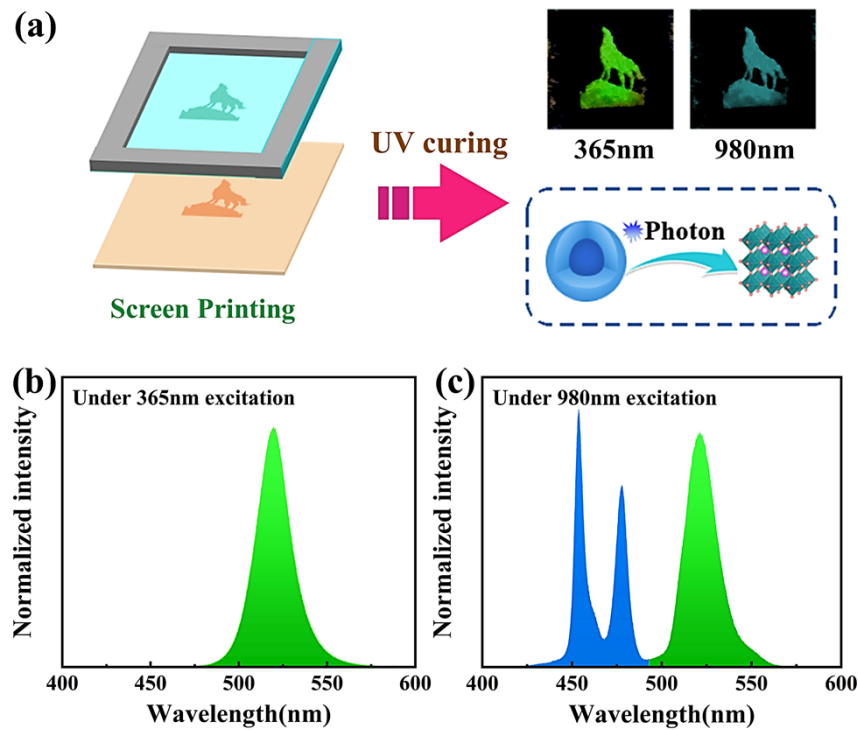


Fig. 7. (a) Schematic illustration of the dual-modal anti-counterfeiting strategy based on the UCNP/CsPbBr₃@UVCR(UCNP/CsPbBr₃=1:0.25). PL spectra of anti-counterfeiting pattern under laser excitation at (b)365 nm and (c)980 nm.

3. Conclusions

In conclusion, we have successfully developed NIR excitable UCNP/CsPbBr₃@UVCR nanocomposites for dual-mode anti-counterfeiting application. The UCNP/CsPbBr₃ are obtained by mixing UCNP with CsPbBr₃ PeQDs which demonstrate excellent upconversion luminescence properties. By changing the different halogen ratios of CsPbX₃ (X = Br/I), multicolor upconversion fluorescence is achieved under NIR excitation. In addition, the time-resolved decay of the exciton recombination is significantly extended from inherent nanoseconds to the milliseconds during the ERA process due to the higher excited levels (¹D₂ and ¹G₄) of Tm³⁺. Through using UCNP as physically existing intermediate energy levels, which breaks the requirement of molecular distance for energy transfer and makes the upconversion more efficient. In short, UCNP/CsPbX₃ has significant upconversion luminescence characteristics with high brightness and multicolor. The combination of the UCNP/CsPbX₃ and UVCR makes UCNP/CsPbX₃ have excellent environmental resistance and full of vitality in the field of anti-counterfeiting. It is expected that the UCNP/CsPbBr₃@UVCR nanocomposites have potential application for information security and encryption.

Funding. High School Science and Technology Funding Planning Project of Shandong Province of China (J18KA222); Natural Science Foundation of Shandong Province (ZR2019MA066, ZR2019MF057); National Natural Science Foundation of China (61905106); Taishan Scholars Project of Shandong Province (tsqn201812098 and ts201511055).

Disclosures. The authors declare no conflicts of interest.

Data availability. No data were generated or analyzed in the presented research.

Supplemental document. See [Supplement 1](#) for supporting content.

References

1. M. R. Carro-Temboury, R. Arppe, T. Vosch, and T. J. Sørensen, "An optical authentication system based on imaging of excitation-selected lanthanide luminescence," *Sci. Adv.* **4**(1), e1701384 (2018).
2. Z. Hu, J. M. M. L. Comeras, H. Park, J. Tang, A. Afzali, G. S. Tulevski, J. B. Hannon, M. Liehr, and S.-J. Han, "Physically unclonable cryptographic primitives using self-assembled carbon nanotubes," *Nat. Nanotechnol.* **11**(6), 559–565 (2016).
3. R. Arppe and T. J. Sørensen, "Physical unclonable functions generated through chemical methods for anti-counterfeiting," *Nat. Rev. Chem.* **1**(4), 0031 (2017).
4. X. Hou, C. Ke, C. J. Bruns, P. R. McGonigal, R. B. Pettman, and J. F. Stoddart, "Tunable solid-state fluorescent materials for supramolecular encryption," *Nat. Commun.* **6**(1), 6884 (2015).
5. K. Jiang, L. Zhang, J. Lu, C. Xu, C. Cai, and H. Lin, "Triple-mode emission of carbon dots: applications for advanced anti-counterfeiting," *Angew. Chem. Int. Ed.* **128**(25), 7347–7351 (2016).
6. Q. Lou, S. Qu, P. Jing, W. Ji, D. Li, J. Cao, H. Zhang, L. Liu, J. Zhao, and D. Shen, "Water-Triggered luminescent "nano-bombs" based on supra-(carbon nanodots)," *Adv. Mater.* **27**(8), 1389–1394 (2015).
7. B. Qin, H. Chen, H. Liang, L. Fu, X. Liu, X. Qiu, S. Liu, R. Song, and Z. Tang, "Reversible photoswitchable fluorescence in thin films of inorganic nanoparticle and polyoxometalate assemblies," *J. Am. Chem. Soc.* **132**(9), 2886–2888 (2010).
8. I. L. Medintz, S. A. Trammell, H. Mattoussi, and J. M. Mauro, "Reversible modulation of quantum dot photoluminescence using a protein-bound photochromic fluorescence resonance energy transfer acceptor," *J. Am. Chem. Soc.* **126**(1), 30–31 (2004).
9. H. Dong, S.-R. Du, X.-Y. Zheng, G.-M. Lyu, L.-D. Sun, L.-D. Li, P.-Z. Zhang, C. Zhang, and C.-H. Yan, "Lanthanide nanoparticles: from design toward bioimaging and therapy," *Chem. Rev.* **115**(19), 10725–10815 (2015).
10. Q. Ma, J. Wang, Z. Li, D. Wang, X. Hu, Y. Xu, and Q. Yuan, "Near-infrared-light-mediated high-throughput information encryption based on the inkjet printing of upconversion nanoparticles," *Inorg. Chem. front* **4**(7), 1166–1172 (2017).
11. C. Zhang, B. Wang, W. Li, S. Huang, L. Kong, Z. Li, and L. Li, "Conversion of invisible metal-organic frameworks to luminescent perovskite nanocrystals for confidential information encryption and decryption," *Nat. Commun.* **8**(1), 1–9 (2017).
12. B. Zhou, B. Shi, D. Jin, and X. Liu, "Controlling upconversion nanocrystals for emerging applications," *Nat. Nanotechnol.* **10**(11), 924–936 (2015).
13. G. Jalani, R. Naccache, D. H. Rosenzweig, L. Haglund, F. Vetrone, and M. Cerruti, "Photocleavable hydrogel-coated upconverting nanoparticles: a multifunctional theranostic platform for NIR imaging and on-demand macromolecular delivery," *J. Am. Chem. Soc.* **138**(3), 1078–1083 (2016).
14. N. M. Idris, M. K. Gnanasamandhan, J. Zhang, P. C. Ho, R. Mahendran, and Y. Zhang, "In vivo photodynamic therapy using upconversion nanoparticles as remote-controlled nanotransducers," *Nat. Med.* **18**(10), 1580–1585 (2012).
15. M. K. G. Jayakumar, N. M. Idris, and Y. Zhang, "Remote activation of biomolecules in deep tissues using near-infrared-to-UV upconversion nanotransducers," *Proc. Natl. Acad. Sci.* **109**(22), 8483–8488 (2012).
16. Y. Zhong, Z. Ma, F. Wang, X. Wang, Y. Yang, Y. Liu, X. Zhao, J. Li, H. Du, and M. Zhang, "In vivo molecular imaging for immunotherapy using ultra-bright near-infrared-IIb rare-earth nanoparticles," *Nat. biotechnol.* **37**(11), 1322–1331 (2019).
17. M. Haase and H. Schäfer, "Upconverting nanoparticles," *Angew. Chem. Int. Ed.* **50**(26), 5808–5829 (2011).
18. B. Chen, W. Kong, Y. Liu, Y. Lu, M. Li, X. Qiao, X. Fan, and F. Wang, "Crystalline hollow microrods for site-selective enhancement of nonlinear photoluminescence," *Angew. Chem. Int. Ed.* **56**(35), 10383–10387 (2017).
19. B. Chen, Y. Liu, Y. Xiao, X. Chen, Y. Li, M. Li, X. Qiao, X. Fan, and F. Wang, "Amplifying excitation-power sensitivity of photon upconversion in a NaYbF₄: Ho nanostructure for direct visualization of electromagnetic hotspots," *J. Phys. Chem. Lett.* **7**(23), 4916–4921 (2016).
20. A. Bagheri, H. Arandiyani, C. Boyer, and M. Lim, "Lanthanide-doped upconversion nanoparticles: emerging intelligent light-activated drug delivery systems," *Adv. Sci.* **3**(7), 1500437 (2016).
21. G. Jalani, V. Tam, F. Vetrone, and M. Cerruti, "Seeing, targeting and delivering with upconverting nanoparticles," *J. Am. Chem. Soc.* **140**(35), 10923–10931 (2018).
22. Y. Fan, L. Liu, and F. Zhang, "Exploiting lanthanide-doped upconversion nanoparticles with core/shell structures," *Nano Today* **25**, 68–84 (2019).
23. B. Chen and F. Wang, "Emerging frontiers of upconversion nanoparticles," *Trends in Chemistry* **2**(5), 427–439 (2020).
24. D. Zhou, D. Liu, W. Xu, X. Chen, Z. Yin, X. Bai, B. Dong, L. Xu, and H. Song, "Synergistic upconversion enhancement induced by multiple physical effects and an angle-dependent anticounterfeit application," *Chem. Mater.* **29**(16), 6799–6809 (2017).
25. S. Cui, L. Tao, W. K. Chan, D. Zhou, Z. Yu, and W. Xu, "Tunable concentration-dependent upconversion and downconversion luminescence in NaYF₄: Yb³⁺, Er³⁺@NaYF₄: Yb³⁺, Nd³⁺ core-shell nanocrystals for a dual-mode anti-counterfeiting imaging application," *Opt. Lett.* **47**(11), 2814–2817 (2022).
26. E. L. Prime and D. H. Solomon, "Australia's plastic banknotes: fighting counterfeit currency," *Angew. Chem. Int. Ed.* **49**(22), 3726–3736 (2010).

27. P. Kumar, J. Dwivedi, and B. K. Gupta, "Highly luminescent dual mode rare-earth nanorod assisted multi-stage excitable security ink for anti-counterfeiting applications," *J. Mater. Chem. C* **2**(48), 10468–10475 (2014).
28. L. Protesescu, S. Yakunin, M. I. Bodnarchuk, F. Krieg, R. Caputo, C. H. Hendon, R. X. Yang, A. Walsh, and M. V. Kovalenko, "Nanocrystals of cesium lead halide perovskites (CsPbX₃, X = Cl, Br, and I): novel optoelectronic materials showing bright emission with wide color gamut," *Nano Lett.* **15**(6), 3692–3696 (2015).
29. G. Nedelcu, L. Protesescu, S. Yakunin, M. I. Bodnarchuk, M. J. Grotevent, and M. V. Kovalenko, "Fast anion-exchange in highly luminescent nanocrystals of cesium lead halide perovskites (CsPbX₃, X = Cl, Br, I)," *Nano Lett.* **15**(8), 5635–5640 (2015).
30. G. Pan, X. Bai, D. Yang, X. Chen, P. Jing, S. Qu, L. Zhang, D. Zhou, J. Zhu, and W. Xu, "Doping lanthanide into perovskite nanocrystals: highly improved and expanded optical properties," *Nano Lett.* **17**(12), 8005–8011 (2017).
31. D. Zhou, D. Liu, G. Pan, X. Chen, D. Li, W. Xu, X. Bai, and H. Song, "Cerium and ytterbium codoped halide perovskite quantum dots: a novel and efficient downconverter for improving the performance of silicon solar cells," *Adv. Mater.* **29**(42), 1704149 (2017).
32. D. Zhou, R. Sun, W. Xu, N. Ding, D. Li, X. Chen, G. Pan, X. Bai, and H. Song, "Impact of host composition, codoping, or tridoping on quantum-cutting emission of ytterbium in halide perovskite quantum dots and solar cell applications," *Nano Lett.* **19**(10), 6904–6913 (2019).
33. W. Zheng, P. Huang, Z. Gong, D. Tu, J. Xu, Q. Zou, R. Li, W. You, J.-C. G. Bünzli, and X. Chen, "Near-infrared-triggered photon upconversion tuning in all-inorganic cesium lead halide perovskite quantum dots," *Nat. Commun.* **9**(1), 3462 (2018).
34. L. Ruan and Y. Zhang, "NIR-excitabile heterostructured upconversion perovskite nanodots with improved stability," *Nat. Commun.* **12**(1), 219 (2021).
35. K. Du, M. Zhang, Y. Li, H. Li, K. Liu, C. Li, J. Feng, and H. Zhang, "Embellishment of upconversion nanoparticles with ultrasmall perovskite quantum dots for full-color tunable, dual-modal luminescence anticounterfeiting," *Adv. Opt. Mater.* **9**(21), 2100814 (2021).
36. M. Rao, J. Fu, X. Wen, B. Sun, J. Wu, X. Liu, and X. Dong, "Near-infrared-excitabile perovskite quantum dots via coupling with upconversion nanoparticles for dual-modal anti-counterfeiting," *New J. Chem.* **42**(15), 12353–12356 (2018).
37. V. Naresh, V. Adusumalli, Y. Park, and N. Lee, "NIR triggered NaYF₄: Yb³⁺, Tm³⁺@ NaYF₄/CsPb(Br_{1-x}/I_x)₃ composite for up-converted white-light emission and dual-modal anti-counterfeiting applications," *Materials Today Chemistry* **23**, 100752 (2022).
38. L. C. Schmidt, A. Pertegás, S. González-Carrero, O. Malinkiewicz, S. Agouram, G. Minguez Espallargas, H. J. Bolink, R. E. Galian, and J. Pérez-Prieto, "Nontemplate synthesis of CH₃NH₃PbBr₃ perovskite nanoparticles," *J. Am. Chem. Soc.* **136**(3), 850–853 (2014).
39. E. J. Juarez-Perez, Z. Hawash, S. R. Raga, L. K. Ono, and Y. Qi, "Thermal degradation of CH₃NH₃PbI₃ perovskite into NH₃ and CH₃I gases observed by coupled thermogravimetry–mass spectrometry analysis," *Energy Environ. Sci.* **9**(11), 3406–3410 (2016).
40. V. Malgras, S. Tominaka, J. W. Ryan, J. Henzie, T. Takei, K. Ohara, and Y. Yamauchi, "Observation of quantum confinement in monodisperse methylammonium lead halide perovskite nanocrystals embedded in mesoporous silica," *J. Am. Chem. Soc.* **138**(42), 13874–13881 (2016).
41. D. N. Dirin, L. Protesescu, D. Trummer, I. V. Kochetygov, S. Yakunin, F. Krumeich, N. P. Stadie, and M. V. Kovalenko, "Harnessing defect-tolerance at the nanoscale: highly luminescent lead halide perovskite nanocrystals in mesoporous silica matrixes," *Nano Lett.* **16**(9), 5866–5874 (2016).
42. Y. Wang, L. Varadi, A. Trinchi, J. Shen, Y. Zhu, G. Wei, and C. Li, "Spray-Assisted Coil–Globule Transition for Scalable Preparation of Water-Resistant CsPbBr₃@ PMMA Perovskite Nanospheres with Application in Live Cell Imaging," *Small* **14**(51), 1803156 (2018).
43. J. Sun, Q. Hua, M. Zhao, L. Dong, Y. Chang, W. Wu, J. Li, Q. Chen, J. Xi, and W. Hu, "Stable ultrathin perovskite/polyvinylidene fluoride composite films for imperceptible multi-color fluorescent anti-counterfeiting labels," *Adv. Mater. Technol-US* **6**(10), 2100229 (2021).
44. V. K. Ravi, G. B. Markad, and A. Nag, "Band edge energies and excitonic transition probabilities of colloidal CsPbX₃ (X = Cl, Br, I) perovskite nanocrystals," *ACS. Energy. Lett.* **1**(4), 665–671 (2016).
45. W. Luo, C. Fu, R. Li, Y. Liu, H. Zhu, and X. Chen, "Er³⁺-doped anatase TiO₂ nanocrystals: Crystal-field levels, excited-state dynamics, upconversion, and defect luminescence," *Small* **7**(21), 3046–3056 (2011).
46. S. Yakunin, J. Chaaban, B. M. Benin, I. Cherniukh, C. Bernasconi, A. Landuyt, Y. Shynkarenko, S. Bolat, C. Hofer, and Y. E. Romanyuk, "Radiative lifetime-encoded unicolor security tags using perovskite nanocrystals," *Nat. Commun.* **12**(1), 981 (2021).
47. F. Wang, R. Deng, J. Wang, Q. Wang, Y. Han, H. Zhu, X. Chen, and X. Liu, "Tuning upconversion through energy migration in core–shell nanoparticles," *Nat. Mater.* **10**(12), 968–973 (2011).
48. J. Ren, X. Dong, G. Zhang, T. Li, and Y. Wang, "Air-stable and water-resistant all-inorganic perovskite quantum dot films for white-light-emitting applications," *New J. Chem.* **41**(22), 13961–13967 (2017).